ACS APPLIED MATERIALS & INTERFACES

Research Article

www.acsami.org

Improved Performance of Organic Light-Emitting Field-Effect Transistors by Interfacial Modification of Hole-Transport Layer/Emission Layer: Incorporating Organic Heterojunctions

Li Song,[†,‡] Yongsheng Hu,[*,†] Nan Zhang,[†] Yantao Li,[†] Jie Lin,[†] and Xingyuan Liu[*,†]

[†]State Key Laboratory of Luminescence and Applications, Changchun Institute of Optics, Fine Mechanics and Physics, Chinese Academy of Sciences, Changchun 130033, China

[‡]University of Chinese Academy of Sciences, Beijing 100049, China

Supporting Information

ABSTRACT: Organic heterojunctions (OHJs) consisting of a strong electron acceptor 1,4,5,8,9,11-hexaazatriphenylene hexacarbonitrile (HAT-CN) and an electron donor N,N′-di(naphthalene-1-yl)-N,N′-diphenyl-benzidine (NPB) were demonstrated for the first time that they can be implemented as effective modification layers between hole transport layer (HTL) and emission layer in the heterostructured organic light-emitting field effect transistors (OLEFETs). The influence of both HAT-CN/NPB junction (npJ) and NPB/HAT-CN junction (pnJ) on the optoelectronic performance of OLEFETs were conscientiously investigated. It is found that both the transport ability of holes and the injection ability of holes into emissive layer can be dramatically improved via the charge transfer of the OHJs and that between HAT-CN and the HTL. Consequently, OLEFETs with pnJ present optimal performance of an external quantum efficiency (EQE) of 3.3% at brightness of 2630 cdm^{-2} and the ones with npJs show an EQE of 4.7% at brightness of 4620 cdm^{-2}. By further utilizing npn OHJs of HAT-CN/NPB/HAT-CN, superior optoelectronic performance with an EQE of 4.7% at brightness of 8350 cdm^{-2} and on/off ratio of 1×10^5 is obtained. The results demonstrate the great practicality of implementing OHJs as effective modification layers in heterostructured OLEFETs.

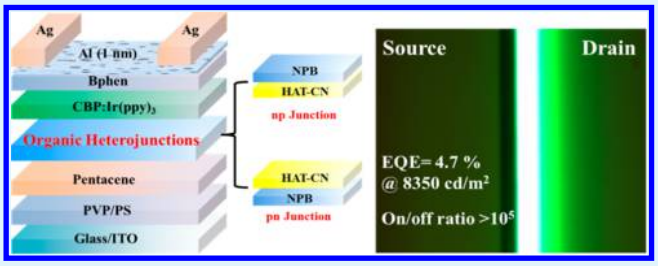

KEYWORDS: *organic heterojunctions, interfacial modification, light-emitting, field effect transistors, charge transfer*

INTRODUCTION

Organic light-emitting field-effect transistor (OLEFET) is a promising low-cost display technology as a result of integrated switching function of field-effect transistors and luminescence function of organic light-emitting devices (OLEDs), which ensure them fascinating applications in the fields of flat panel displays, sensors, optical communication, and potentially, electrically driven organic lasers.[1−8] During the past decade, great efforts have been made to improve the performance of the OLEFETs such as developing or adopting organic materials with high carrier mobilities,[9,10] optimizing electrode and device structures,[11−14] employing interfacial doping techniques, and so on.[15] Although both the optical and electrical performance of the OLEFETs has a very big enhancement, there is still a large gap from practical applications.

Generally, heterostructured OLEFETs[16−21] consisting of an emissive layer (EML) and a p-type and/or a n-type carrier transport layer (CTL) rather than a single active layer[22−24] bring high flexibility of structure design and increase the potential in achieving better overall performance especially in on/off ratio due to their advantages of that (1) CTL materials with high carrier mobilities and EML materials with high photoluminescene quantum yield (PLQY) can be simultaneously adopted; (2) exciton formation and carrier accumulation zones are restricted in different layers leading to reduced charge-exciton quenching phenomenon. However, owing to different energy levels of EML, CTL, and the source/drain (S/D) electrodes, when incorporating CTL with high carrier mobility and EML with high PLQY in an OLEFET, often there are great energy barriers among the interface of them, which will cause insufficient carrier injection from the S/D electrodes or inefficient carrier migration between the organic active layers, and then accounts for the difficulty in obtaining high external quantum efficiency (EQE) and high brightness simultaneously for most heterostructured OLEFETs. Many methods such as asymmetric S/D electrodes[25] and interfacial modification for the electrode/active layer[26] and the insulator/active layer[27] have been studied to overcome this conflict. However, attempts on the interfacial modification between organic active layers have been rarely reported.

Distinct from the inorganic pn junctions that are usually depleted, organic heterojunctions (OHJs) composed of a p-

Received: March 4, 2016
Accepted: May 24, 2016
Published: May 24, 2016

DOI: 10.1021/acsami.6b02618
ACS Appl. Mater. Interfaces 2016, 8, 14063−14070

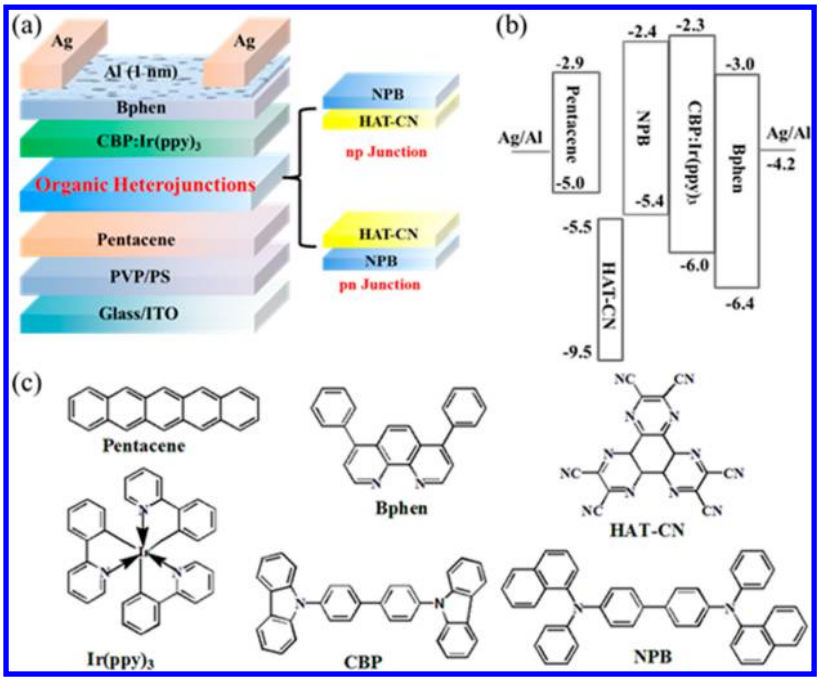

Figure 1. (a) Schematic of the heterostructured OLEFETs, the OHJs include HAT-CN/NPB (npJ) and NPB/HAT-CN (pnJ). (b) Energy-level diagram of organic materials. (c) Molecular structures of the active materials used.

type organic semiconductor (OSC) and a n-type OSC are usually accumulated with high conductivity, which enables them wide applications in organic electronics.[28−30] Namely, OHJ can be considered as an effective charge generation layer in tandem OLEDs, where the generated electrons and holes can inject from the opposite direction into the two sub-OLEDs, respectively, and recombine with the carriers injected from the electrodes, leading to great improvement for characteristics such as brightness and current efficiency.[30,31]

Here, we demonstrate for the first time that OHJs can be utilized as an efficient modification layer between a hole transport layer (HTL) and an EML for heterostructured OLEFETs. OHJs of both pn junction and np junction were carefully investigated. It is found that the charge generation from the OHJs and the charge transfer between the n-type OSC of OHJs and the HTL can significantly enhance both the hole transport ability of the HTL and the hole injection ability into the EML, which accounts for almost 1 order of magnitude increase for EQE with high brightness. By further implementing npn junction as the modification layer, state-of-the-art performance with EQE of 4.7% at brightness of 8350 cdm^{-2} as well as the on/off ratio >1 × 10^5 was obtained. The novel and efficient OHJ interfacial modification enables much flexibility in selection of the active materials and avoids using sophisticated asymmetric S/D electrodes, which is of great significance for realizing high-performance, simple-process, and multicolor OLEFETs in the future.

RESULTS AND DISCUSSION

Three kinds of device structures are involved in this work including two with different OHJ modifications and a control one without modification. Figure 1a shows the two OHJ modified device structures. Figure 1b, c gives the energy levels and molecular structures of the organic materials used in this work, respectively. The OLEFETs were fabricated by using poly-4-vinylphenol (PVP, 420 nm)/polystyrene (PS, 30 nm) as the dielectric on ITO substrate. Pentacene (12 nm) was used as the HTL because of its high hole mobility. The OHJs were constructed by N,N′-di(naphthalene-1-yl)-N,N′-diphenyl-benzidine (NPB, 10 nm) and 1,4,5,8,9,11-hexaazatriphenylene hexacarbonitrile (HAT-CN). According to the deposition sequence, we define HAT-CN/NPB as the np junction (npJ) and NPB/HAT-CN as the pn junction (pnJ). The EML is 4,4′-bis(carbazol-9-yl)biphenyl (CBP): Fac-tris(2-phenylpyridinato)iridium(III) ($Ir(ppy)_3$) (20 nm, 6 wt %), a typical host−guest matrix used in OLEDs. Bathophenanthroline (Bphen, 14 nm) was used as the electron-injection layer and hole-blocking layer due to the suitable highest occupied molecular orbital (HOMO) level (−6.4 eV) (see Figure 1b). Ag (50 nm) was used as the S/D electrodes, before which an ultrathin layer of Al (1 nm) was inserted to further promote the electron injection as reported in the OLEDs.[32,33]

It is known that charge transfer will probably occur when HAT-CN contacts with suitable HOMO-level p-type OSCs:[34,35] the electrons in the HOMO level of the p-type OSC will transfer to the lowest unoccupied molecular orbital (LUMO) level of HAT-CN, leaving holes in the HOMO level of the p-type OSC.[36] We first confirm the existence of charge transfer between HAT-CN and NPB. Figure 2a shows the UV−vis−NIR absorption spectra of HAT-CN, NPB, and HAT-CN-doped NPB (50 mol % HAT-CN) films. A red-shift absorption band occurred with a newly emerged peak at around 800 nm in the blend film, which is a sign of the charge transfer between HAT-CN and NPB.[34] Furthermore, considering that HAT-CN was deposited on the top of pentacene film for npJ device, charge transfer may also occur between HAT-CN and pentacene because of the low HOMO level of pentacene. Figure 2b gives the UV−vis−NIR absorption spectra of pentacene, HAT-CN, and HAT-CN-doped pentacene (50 mol % HAT-CN) films. The red-shift peak around 950 nm in the HAT-CN-doped pentacene film indicates that the charge transfer phenomenon also exists between HAT-CN and pentacene.

DOI: 10.1021/acsami.6b02618
ACS Appl. Mater. Interfaces 2016, 8, 14063−14070

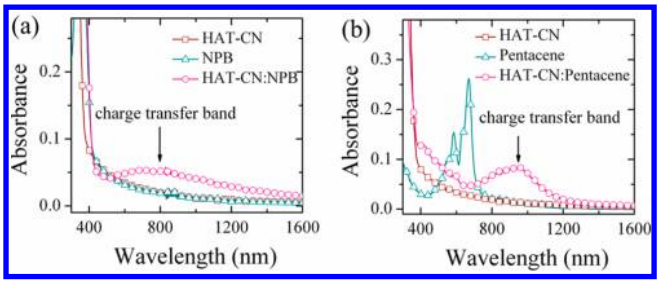

Figure 2. (a) UV−vis−NIR absorption spectra of NPB film (60 nm), HAT-CN film (60 nm), and HAT-CN-doped NPB film (60 nm, 50 mol % HAT-CN). (b) UV−vis−NIR absorption spectra of pentacene film (60 nm), HAT-CN film (60 nm), and HAT-CN-doped pentacene film (60 nm, 50 mol % HAT-CN).

We have investigated npJ and pnJ devices with different thickness of HAT-CN and found that the maximum drain current (I_{DS}) for both devices increases significantly with the increasing of the thickness of HAT-CN, as is shown in Figures S1a and S2a. Figure S3 shows the atomic force microscope (AFM) images for 0, 1, 2, and 4 nm HAT-CN films grown on top of pentacene and NPB films. It can be seen that the nucleation of HAT-CN on both pentacene and NPB becomes denser and larger as the thickness of HAT-CN increases, which means larger contact area. The increasing maximum I_{DS} for thicker HAT-CN probably resulted from the better contact because stronger charge transfer can occur between HAT-CN and pentacene or NPB. The hole mobility calculated in the saturated region of the transfer curves also increases accordingly from 0.026 to 0.43 $cm^2\ V^{-1}\ s^{-1}$ for npJ and from 0.13 to 1.28 $cm^2\ V^{-1}\ s^{-1}$ for pnJ, respectively, as listed in Table 1. The elevated hole mobility is probably resulted from the filling of the charge traps of pentacene by the extra charges[37−39] generated from the charge transfer between HAT-CN and pentacene or NPB.

The light emission becomes more intense as the drain current increases, which is in agreement with that for unipolar OLEFETs in the literature.[40,41] The maximum brightness of 9350 cdm^{-2} and 14290 cdm^{-2} is obtained for npJ and pnJ devices with 4 nm HAT-CN, respectively (see Figures S1b and S2b). However, the EQE represents much decrease from 5.2 to 3.7% and 3.3 to 1.2% for npJ and pnJ devices, respectively, as HAT-CN increases from 1 to 4 nm. The decrease of EQE is probably attributed to the overbalance of holes and electrons resulting from the greatly increased hole current. Considering the better EQE at relatively high brightness (>2500 cdm^{-2}), we will focus on npJ device with 2 nm HAT-CN and pnJ device with 1 nm HAT-CN in the following discussion.

Figure 3a presents the electrical and optical transfer curves of the control device, npJ device and pnJ device at drain to source voltage V_{DS}= −100 V. All the devices exhibit typical p-type characteristic, which can be also verified by their output curves in Figures S4ac and S5a, where distinct linear and saturation regimes can be found. The maximum I_{DS} and hole mobility for control device are ∼3 μA and 0.002 $cm^2\ V^{-1}\ s^{-1}$, respectively. Remarkably, the maximum I_{DS} for both npJ device and pnJ device reaches above 100 μA, which is more than 30 times higher than that of the control device. The hole mobilities also increase to 0.15 $cm^2\ V^{-1}\ s^{-1}$ and 0.13 $cm^2\ V^{-1}\ s^{-1}$ for npJ device and pnJ device, respectively. The significant enhancement of hole transport ability for OHJs devices can be attributed to the charge transfer processes under the source electrode. For better interpretation, we present the operating mechanism for common unipolar OLEFETs, i.e., the control device, in Figure 3c-2, which contains: (a) hole injection from the source electrode into pentacene via the above Bphen/CBP:$Ir(ppy)_3$ layers; (b) hole accumulation and transportation along the interface of dielectric/pentacene toward the drain electrode due to the field effect; (c) hole injection into CBP followed by exciton formation with the electrons injected from the drain electrode; (d) exciton recombination radiation and light emission under the drain electrode. The above processes indicate that the large energy barrier between the work function of Ag and the HOMO level of pentacene as well as the hole blocking effect of Bphen/CBP:$Ir(ppy)_3$ under the source electrode is mainly responsible for the small hole current in the control device. According to Sun's investigation,[42] the electrons and holes generated from the charge transfer of an OHJ can separate effectively when the OHJ is biased under reverse electric field (electric field directs from HAT-CN to p-type OSCs). As for the pnJ device, when operating in the hole accumulation mode (gate to source voltage $V_{GS} < 0$, $V_{DS} < 0$), the electric field beneath the source electrode points primarily from HAT-CN to NPB, as shown in Figure 3c-1. Assisted by the electric field, extra holes can be generated in the HOMO level of NPB and successively inject into pentacene under the source electrode. The generated holes together with the holes injected directly from the source electrode form the current channel, leading to the increase of the I_{DS}. However, the direction of electric field under the source electrode is not conducive to the above charge transfer process with regard to the npJ device. Fortunately, the OHJ formed between HAT-CN and pentacene would be biased under reverse electric field, which enables more holes generated in the HOMO level of

Table 1. Summary of the Optical and Electrical Performance for OLEFETs with Different Structures[a]

OHJs	thickness (nm)	max brightness (cdm^{-2})	EQE at max brightness (%)	max emission zone width (μm)	recombination efficiency at max brightness (%)	on/off ratio	mobility ($cm^2\ V^{-1}\ s^{-1}$)
control		10 ± 1	0.46 ± 0.05	60	2.6 ± 0.3	1×10^4	0.0024
HAT/NPB (npJ)	1/10	1610 ± 50	5.2 ± 0.3	100	29.5 ± 1.7	1×10^4	0.026
	2/10	4620 ± 80	4.7 ± 0.3	140	26.7 ± 1.7	1×10^5	0.15
	4/10	9350 ± 200	3.7 ± 0.3	140	21.0 ± 1.7	1×10^5	0.43
NPB/HAT (pnJ)	10/1	2630 ± 80	3.3 ± 0.2	120	18.8 ± 1.1	1×10^5	0.13
	10/2	12730 ± 300	2.2 ± 0.1	120	12.5 ± 0.6	1×10^5	1.16
	10/4	14290 ± 300	1.2 ± 0.1	120	6.8 ± 0.6	1×10^5	1.28
HAT/NPB/HAT (npnJ)	2/10/1	8350 ± 200	4.7 ± 0.3	140	26.5 ± 1.7	1×10^5	0.66

[a]Average values for at least five devices, errors given are the standard deviation of the results.

DOI: 10.1021/acsami.6b02618
ACS Appl. Mater. Interfaces 2016, 8, 14063−14070

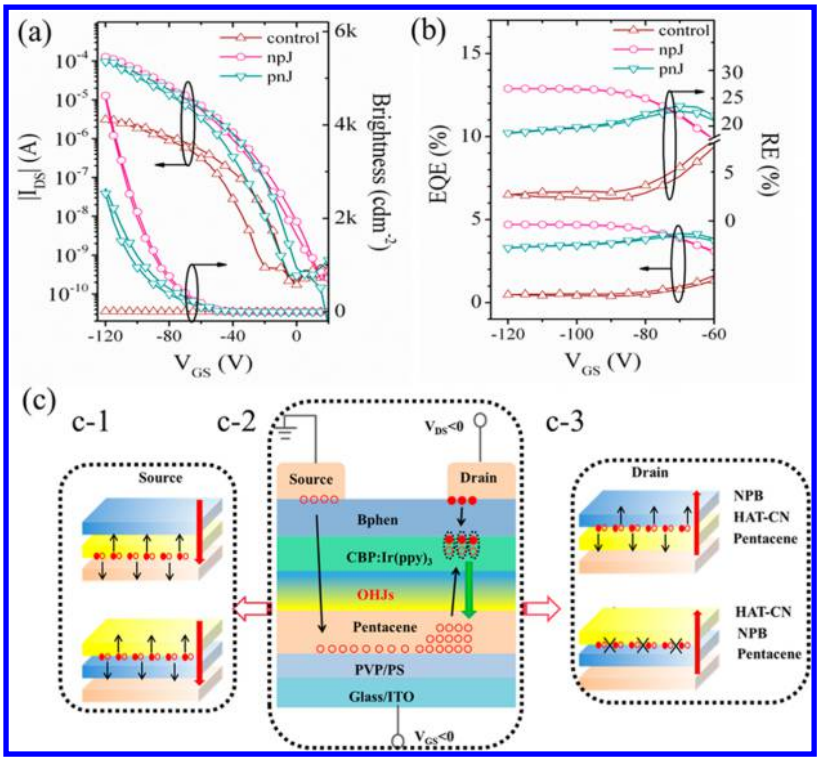

Figure 3. (a) Electrical and optical transfer characteristics (V_{DS} = −100 V) for control, npJ, and pnJ devices. (b) EQE as well as exciton recombination efficiency corresponding to the transfer characteristics. (c) Schematic representations of the carrier injection and transport (C-2) along with the charge transfer processes beneath the source electrode (C-1) and the drain electrode (C-3) for both npJ device and pnJ device. The red arrows in C-1 and C-3 denote the directions of the electric field. The green arrow in C-2 denotes the light-emission direction. The " × " in the bottom part of C-3 means that the charge transfer between NPB/HAT-CN is unlikely to occur under the drain electrode.

pentacene and accumulated in the channel, accounting for the increase in I_{DS} in the npJ device. It is notable that the introduction of OHJs makes unconspicuous influence on the off current, hence the on/off ratios increase more than 1 order of magnitude to 1 × 10^5 for both npJ and pnJ devices.

The optical characteristics also agree well with those for unipolar OLEFETs as the light emission intensity increases with the increasing of the drain current and the emission zone mainly exists beneath the electron injection electrode (drain electrode). Figure S6a displays the optical microphotographs of the emission zones for the npJ device when V_{DS} = −100 V and V_{GS} varies from −70 V to −120 V with step of −10 V. We also profiled the emission intensity across the device channel and partial electrodes (Figure S6b) to obtain accurate emission zone widths (full width at half-maximum, fwhm) based on the given microphotographs. As the V_{GS} increases negatively, the light emission area extends gradually underneath the electron injection electrode concomitant with the progressively enhanced brightness, indicating more holes are accumulating under the drain electrode.[43] The maximum width of the emission zone is approximately 140 μm, which is potentially useful for OLEFET-based display technology where large aperture ratios with fine pixels are desired.[44,45] The maximum widths of the emission zone for other devices are listed in Table 1 addressed by the same method. The brightness for all the three devices increases with the increasing of respective drain current. The maximum brightness for npJ and pnJ devices reaches ∼4620 cd m^{-2} and ∼2630 cd m^{-2}, respectively, which are hundreds of times higher than that of the control device (∼10 cd m^{-2}).

The EQE related to the transfer curves is shown in Figure 3b. The EQE was calculated from the brightness, electroluminescent (EL) spectra (see Figure S6c), and drain current assuming Lambertian emission. The EQE for the control device is only 0.46% at the maximum brightness of 10 cd m^{-2}. The EQE for npJ device approaches to 4.7% at brightness up to 4620 cd m^{-2} and exhibits almost no degradation when V_{GS} changes from −90 V to −120 V. To the best of our knowledge, such EQE along with the high brightness are the best results for molecular OLEFETs. The EQE for pnJ device is 3.3% at the maximum brightness of ∼2630 cd m^{-2}. Figure S7 also presents the EQE versus drain current and EQE versus brightness for different devices. The variations of EQE with the change of drain current or brightness seem identical for different devices: for drain current higher than 1 μA or brightness higher than 5 cd m^{-2}, the EQE first increases as the drain current (brightness) gets higher and a maximum EQE appears, then the EQE drops in certain degrees for different devices, which is known as efficiency roll-off in OLEDs. It is also worth noting that the abnormal value of EQE at low current (∼1 × 10^{-7} A) or low brightness (<5 cd m^{-2}) for the control device is probably due to the inaccurate estimation of the emission area because the light intensity is rather weak.

A deep insight into the origin of the improved EQE can be given by the formular[43]

$$\Phi_{EQE} = \Phi_{out}\Phi_{spin}\Phi_{PL}\Phi_{capture} \quad (1)$$

where Φ_{EQE} is the calculated EQE, Φ_{out} is the outcoupling efficiency, Φ_{spin} is a factor to take account of spin statistics, Φ_{PL} is the PLQY of the emitting material, and $\Phi_{capture}$ is the recombination efficiency (RE) determined by the capture of

DOI: 10.1021/acsami.6b02618
ACS Appl. Mater. Interfaces 2016, 8, 14063−14070

hole and electrons. Φ_{out} can be assumed to be 20% for common OLEDs,[46] whereas $\Phi_{spin} \approx 1$ because phosphorescent emitting material is used,[47] and Φ_{PL} is ~88% obtained by the experiment. The major difference in EQE comes from the $\Phi_{capture}$. For intuitive comparison, we also plot the RE versus V_{GS} in Figure 3b. The RE for the control device is only 2.6% while that for npJ and pnJ devices reaches 26.7 and 18.8%, respectively, at their respective maximum brightness. The low RE for the control device arises from the large hole injection barrier (~1 eV) between pentacene and CBP (see Figure 1b), which results in poor hole injection efficiency into CBP under the drain electrode. The use of NPB will facilitate the hole injection by reducing the barrier, thus promoting the exciton RE, which can be verified by the lower exciton RE (~9.1%) and brightness (~1500 cd m^{-2}) when the NPB is removed for the npJ device (see Figure S8). As for the difference of exciton RE between the npJ device and the pnJ device, we conjecture that the charge transfer between HAT-CN and NPB under the drain electrode for npJ device plays a crucial role. Because the electric field under the drain electrode of the npJ device directs from HAT-CN to NPB, the charge transfer between HAT-CN and NPB could happen (see Figure 3c-3); therefore, the hole injection into the EML would be more efficient, leading to the higher exciton RE.

Two types of hole-only diode-structured devices with different thickness of HAT-CN were fabricated to further clarify the effect of the charge transfer of the OHJs on the changes of the hole current under different electric fields: ITO/pentacene/HAT-CN (x nm)/NPB/Au (device A), ITO/pentacene/NPB/HAT-CN (x nm)/Au (device B). The thickness of pentacene and NPB are 80 and 150 nm, respectively. Figure 4 depicts the relationship between the current density and voltage when ITO and Au is set as the anode, respectively. As the thickness of HAT-CN becomes thicker, the current density for device A represents a remarkable increase when Au is set as the anode (Figure 4a) while it almost keeps the same when ITO is set as the anode (Figure 4b). This indicates that the charge transfer of NPB/HAT-CN is more likely to happen when biased at a reverse electric field, which is consistent with the conclusion that the drain current enhancement for the pnJ device is originated from the charge transfer between HAT-CN and NPB under the source electrode. Similarly, as the thickness of HAT-CN increases, the current density for device B continuously increases when ITO is set as the anode (Figure 4d). This is also attributed to the reverse bias condition of HAT-CN/NPB, which is the case under the drain electrode for the npJ device. The current density of device B also shows an enhancement as the thickness of HAT-CN increases when Au is set as the anode (Figure 4c) indicating that the charge transfer of HAT-CN/pentacene can also promote the hole current under a reverse bias, which agrees well with that under the source electrode for npJ device.

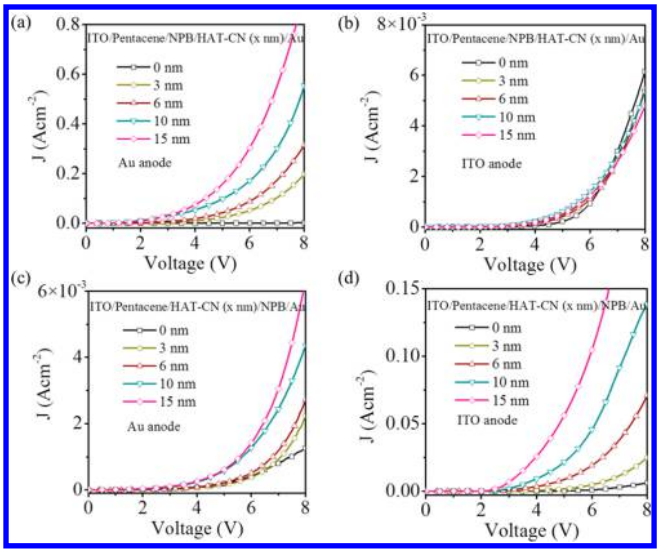

Figure 4. Current density versus voltage for hole-only devices with different structures: ITO/pentacene/NPB/HAT-CN (x nm)/Au (device A), ITO/pentacene/HAT-CN (x nm)/NPB/Au (device B). (a, c) Au is set as the anode and (b, d) ITO is set as the anode. The thickness of pentacene and NPB are 80 and 150 nm, respectively. The thickness of HAT-CN varies from 0 to 15 nm.

To take advantage of these charge transfer processes completely, we designed and developed an OLEFET with HAT-CN (2 nm)/NPB (10 nm)/HAT-CN (1 nm) (npnJ) as the OHJ modification layer. Figure 5a shows the electrical and optical transfer characteristics for V_{DS}= −100 V. The npnJ device presents higher drain current (also see the output curves in Figure S5d) in comparison with those of the npJ and pnJ devices (see Figure 3a) under identical V_{GS} bias because charge transfer of HAT-CN/NPB as well as pentacene/HAT-CH occur concurrently under the source electrode. The well-maintained high RE (Figure 5b) associated with the high brightness confirms the favorable promotion of the hole injection into CBP by virtue of the charge transfer of HAT-CN/NPB under the drain electrode. The superior performance with EQE of 4.7% at brightness of 8350 cd m^{-2} and on/off ratio of 1 × 10^5 holds great promise for practical applications especially in OLEFET-based display technology. Though the operation voltages are quite high for current devices, methods such as adopting high k insulating materials, shortening the channel length, modifying charge transport layer with low defects and lowering the barriers between the active layers would be beneficial in reducing the operation voltages of the devices.[48−51] Moreover, considering the insufficient injection and transport of the electrons, the electrode induced photon absorption and possible metal-exciton quenching, better performance of EQE as well as brightness could be expected by doping the electron-injection layer and adopting electron transport layer with comparable mobility to the HTL.[52]

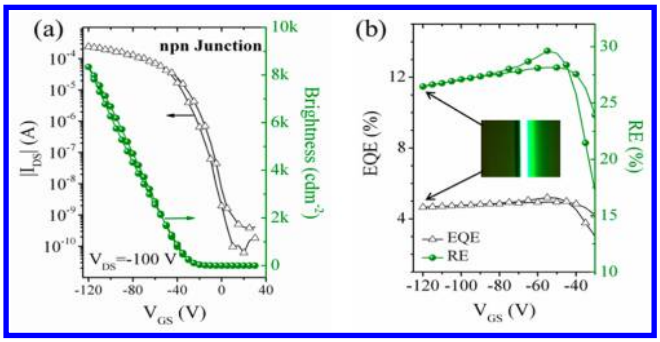

Figure 5. (a) Electrical and optical transfer characteristics (V_{DS} = −100 V) for npnJ device. (b) EQE and exciton recombination efficiency corresponding to the transfer characteristics. Inset is the optical microphotoscopy of the npnJ device at V_{DS} = −100 V and V_{GS} = −120 V.

DOI: 10.1021/acsami.6b02618
ACS Appl. Mater. Interfaces 2016, 8, 14063−14070

CONCLUSION

In summary, we have demonstrated that the OHJs consisted of HAT-CN and NPB can be an efficient interfacial modification layer between the HTL and the EML of herterostructured OLEFETs. The hole transport ability in the HTL and the hole injection ability into the EML can be greatly enhanced as a result of the charge transfer processes associated with the adoption of OHJs with both npJ and pnJ. State-of-the-art performance with EQE of 4.7% at brightness of 8350 cd m^{-2} with on/off ratio of 1×10^5 was achieved by further modifying with npn OHJ of HAT-CN/NPB/HAT-CN. The greatly improved performance afforded by incorporating OHJ modifications manifests the importance of the interfacial modification between the active layers for herterostructured OLEFETs. The use of OHJs therefore also provide an innovative route to realize high-performance, multicolored OLEFETs because more alternative charge transport materials with high mobility and emissive materials with high PLQY can be available without much apprehension of the energy barriers.

EXPERIMENTAL SECTION

Device Fabrication. The PVP solution was prepared with poly(4-vinylphenol) and poly(melamine-*co*-formaldehyde) (2:1 wt %) dissolved in propylene glycol monomethyl ether acetate (PGMEA) (90 mg/mL). The PVP solution was spun coated (30 s at 3000 rpm) onto the cleaned indium tin oxide/glass substrates and then annealed at 200 °C for 1 h to get the first 420 nm dielectric layer. The polystyrene dissolved in toluene (6 mg/mL) was successively spin coated (30 s at 3000 rpm) on PVP and annealed at 85 °C for 1 h. Pentacene, HAT-CN, NPB, CBP: $Ir(ppy)_3$, Bphen and Al were successively thermal evaporated with the rate of 0.2, 0.1, 0.2, 2, 0.2, and 0.2 Å/s, respectively. Ag was thermally deposited through a shadow mask with channel length and width of 45 and 3000 μm, respectively. For fabrication of the hole-only devices, pentacene (80 nm), HAT (0, 3, 6, 10, 15 nm), NPB (150 nm) and Au (50 nm) were thermally evaporated onto the ITO substrates at rates of 1, 1, 2, 5 Å/s, respectively. Organic films of pentacene (60 nm, 1 Å/s), NPB (60 nm, 1 Å/s), HAT-CN (60 nm, 1 Å/s), HAT-CN-doped-pentacene (60 nm, 50% mol HAT-CN, 1 Å/s), and HAT-CN-doped-NPB (60 nm, 50% mol HAT-CN, 1 Å/s) were thermally evaporated on the quartz substrates for the UV−vis−NIR absorption spectra characterization. The thickness and evaporation rates of the organic materials as well as the electrodes were monitored by quartz-crystal oscillators and calibrated ex situ using a surface profiler (Ambios XP-1). The OLEFETs were encapsulated with UV glue in the glovebox (H_2O, O_2 < 0.1 ppm) before testing.

Device Characterization. The electrical characteristics were performed by Keithley 4200 SCS at room temperature under air ambient. The photocurrent was recorded by HAMAMATSU S1336 photodiode. The optical images were captured by Olympus BX51TRF CCD microscope. The electroluminescence spectra were measured by AvaSpec-ULS2048L fiber spectrometer. The absorption spectra were recorded by Shimadzu UV-3101PC UV−vis−NIR spectrophotometer. Absolute fluorescent quantum yield measurements were performed with a calibrated integrating sphere on an Edinburgh FLS920 spectrometer. The atomic force microscopy (AFM) measurement was performed on a Shimadzu SPM-9700. The carrier mobilities were calculated by the formula for the saturation regime: $I_{DS} = \mu C_i(W/2L)(V_{GS} - V_T)^2$, (where μ is the field-effect mobility, C_i is the gate dielectric capacitance density, V_T is the threshold voltage, and W and L are the channel width and length, respectively). The photocurrent was collected from the ITO side. The brightness was calculated by comparing the photocurrent with a standard OLED of known brightness (1000 cdm^{-2}) and emission area (3 mm × 1 mm) with structure of ITO/NPB/CBP:$Ir(ppy)_3$/Bphen/LiF/Al. The EQE was calculated from the brightness, the drain current, and the EL emission spectrum assuming Lambertian emission.

ASSOCIATED CONTENT

Supporting Information

The Supporting Information is available free of charge on the ACS Publications website at DOI: 10.1021/acsami.6b02618.

Optical and electrical characteristics for different OLEFETs, AFM, microphotographs (PDF)

AUTHOR INFORMATION

Corresponding Authors

*E-mail: huyongsheng@ciomp.ac.cn.
*E-mail: liuxy@ciomp.ac.cn.

Notes

The authors declare no competing financial interest.

ACKNOWLEDGMENTS

This work was supported by the CAS Innovation Program, and the National Natural Science Foundation of China through Grant 6140031454, and Project supported by State Key Laboratory of Luminescence and Applications.

REFERENCES

(1) Cicoira, F.; Santato, C. Organic Light Emitting Field Effect Transistors: Advances and Perspectives. *Adv. Funct. Mater.* **2007**, *17*, 3421−3434.

(2) Zaumseil, J.; Sirringhaus, H. Electron and Ambipolar Transport in Organic Field-Effect Transistors. *Chem. Rev.* **2007**, *107*, 1296−1323.

(3) Bisri, S. Z.; Piliego, C.; Gao, J.; Loi, M. A. Outlook and Emerging Semiconducting Materials for Ambipolar Transistors. *Adv. Mater.* **2014**, *26*, 1176−1199.

(4) Bürgi, L.; Turbiez, M.; Pfeiffer, R.; Bienewald, F.; Kirner, H.-J.; Winnewisser, C. High-Mobility Ambipolar near-Infrared Light-Emitting Polymer Field-Effect Transistors. *Adv. Mater.* **2008**, *20*, 2217−2224.

(5) Hotta, S.; Yamao, T.; Bisri, S. Z.; Takenobu, T.; Iwasa, Y. Organic Single-Crystal Light-Emitting Field-Effect Transistors. *J. Mater. Chem. C* **2014**, *2*, 965−980.

(6) Muccini, M.; Koopman, W.; Toffanin, S. The Photonic Perspective of Organic Light-Emitting Transistors. *Laser Photonics Rev.* **2012**, *6*, 258−275.

(7) Melzer, C.; von Seggern, H. Organic Electronics Enlightened Organic Transistors. *Nat. Mater.* **2010**, *9*, 470−472.

(8) Takenobu, T.; Bisri, S. Z.; Takahashi, T.; Yahiro, M.; Adachi, C.; Iwasa, Y. High Current Density in Light-Emitting Transistors of Organic Single Crystals. *Phys. Rev. Lett.* **2008**, *100*, 066601.

(9) Schidleja, M.; Melzer, C.; von Seggern, H. Electroluminescence from a Pentacene Based Ambipolar Organic Field-Effect Transistor. *Appl. Phys. Lett.* **2009**, *94*, 123307.

(10) Schidleja, M.; Melzer, C.; von Seggern, H. Investigation of Charge-Carrier Injection in Ambipolar Organic Light-Emitting Field-Effect Transistors. *Adv. Mater.* **2009**, *21*, 1172−1176.

(11) Sakanoue, T.; Fujiwara, E.; Yamada, R.; Tada, H. Preparation of Organic Light-Emitting Field-Effect Transistors with Asymmetric Electrodes. *Chem. Lett.* **2005**, *34*, 494−495.

(12) Swensen, J. S.; Soci, C.; Heeger, A. J. Light Emission from an Ambipolar Semiconducting Polymer Field-Effect Transistor. *Appl. Phys. Lett.* **2005**, *87*, 253511.

(13) Di, C.-a.; Yu, G.; Liu, Y.; Xu, X.; Wei, D.; Song, Y.; Sun, Y.; Wang, Y.; Zhu, D. Organic Light-Emitting Transistors Containing a Laterally Arranged Heterojunction. *Adv. Funct. Mater.* **2007**, *17*, 1567−1573.

(14) Zaumseil, J.; Donley, C. L.; Kim, J.-S.; Friend, R. H.; Sirringhaus, H. Efficient Top-Gate, Ambipolar, Light-Emitting Field-Effect Transistors Based on a Green-Light-Emitting Polyfluorene. *Adv. Mater.* **2006**, *18*, 2708−2712.

(15) Nakanotani, H.; Saito, M.; Nakamura, H.; Adachi, C. Tuning of Threshold Voltage by Interfacial Carrier Doping in Organic Single

DOI: 10.1021/acsami.6b02618
ACS Appl. Mater. Interfaces 2016, 8, 14063−14070

Crystal Ambipolar Light-Emitting Transistors and Their Bright Electroluminescence. *Appl. Phys. Lett.* **2009**, *95*, 103307.
(16) Dinelli, F.; Capelli, R.; Loi, M. A.; Murgia, M.; Muccini, M.; Facchetti, A.; Marks, T. J. High-Mobility Ambipolar Transport in Organic Light-Emitting Transistors. *Adv. Mater.* **2006**, *18*, 1416−1420.
(17) Capelli, R.; Toffanin, S.; Generali, G.; Usta, H.; Facchetti, A.; Muccini, M. Organic Light-Emitting Transistors with an Efficiency That Outperforms the Equivalent Light-Emitting Diodes. *Nat. Mater.* **2010**, *9*, 496−503.
(18) Seo, H.-S.; Kim, D.-K.; Oh, J.-D.; Shin, E.-S.; Choi, J.-H. Organic Light-Emitting Field-Effect Transistors Based Upon Pentacene and Perylene. *J. Phys. Chem. C* **2013**, *117*, 4764−4770.
(19) Kajii, H.; Tanaka, H.; Kusumoto, Y.; Ohtomo, T.; Ohmori, Y. In-Plane Light Emission of Organic Light-Emitting Transistors with Bilayer Structure Using Ambipolar Semiconducting Polymers. *Org. Electron.* **2015**, *16*, 26−33.
(20) Ullah, M.; Tandy, K.; Yambem, S. D.; Aljada, M.; Burn, P. L.; Meredith, P.; Namdas, E. B. Simultaneous Enhancement of Brightness, Efficiency, and Switching in Rgb Organic Light Emitting Transistors. *Adv. Mater.* **2013**, *25*, 6213−6218.
(21) Yamada, K.; Yamao, T.; Hotta, S. Light-Emitting Field-Effect Transistors Having Combined Organic Semiconductor and Metal Oxide Layers. *Adv. Mater.* **2013**, *25*, 2860−2866.
(22) Komori, T.; Nakanotani, H.; Yasuda, T.; Adachi, C. Light-Emitting Organic Field-Effect Transistors Based on Highly Luminescent Single Crystals of Thiophene/Phenylene Co-Oligomers. *J. Mater. Chem. C* **2014**, *2*, 4918−4921.
(23) Nakanotani, H.; Saito, M.; Nakamura, H.; Adachi, C. Emission Color Tuning in Ambipolar Organic Single-Crystal Field-Effect Transistors by Dye-Doping. *Adv. Funct. Mater.* **2010**, *20*, 1610−1615.
(24) Hsu, B. B. Y.; Duan, C.; Namdas, E. B.; Gutacker, A.; Yuen, J. D.; Huang, F.; Cao, Y.; Bazan, G. C.; Samuel, I. D. W.; Heeger, A. J. Control of Efficiency, Brightness, and Recombination Zone in Light-Emitting Field Effect Transistors. *Adv. Mater.* **2012**, *24*, 1171−1175.
(25) Tandy, K.; Ullah, M.; Burn, P. L.; Meredith, P.; Namdas, E. B. Unlocking the Full Potential of Light Emitting Field-Effect Transistors by Engineering Charge Injection Layers. *Org. Electron.* **2013**, *14*, 2953−2961.
(26) Seo, J. H.; Namdas, E. B.; Gutacker, A.; Heeger, A. J.; Bazan, G. C. Solution-Processed Organic Light-Emitting Transistors Incorporating Conjugated Polyelectrolytes. *Adv. Funct. Mater.* **2011**, *21*, 3667−3672.
(27) Hsu, B. B. Y.; Seifter, J.; Takacs, C. J.; Zhong, C.; Tseng, H.-R.; Samuel, I. D. W.; Namdas, E. B.; Bazan, G. C.; Huang, F.; Cao, Y.; Heeger, A. J. Ordered Polymer Nanofibers Enhance Output Brightness in Bilayer Light-Emitting Field-Effect Transistors. *ACS Nano* **2013**, *7*, 2344−2351.
(28) Chen, Y.; Tian, H.; Geng, Y.; Chen, J.; Ma, D.; Yan, D.; Wang, L. Organic Heterojunctions as a Charge Generation Layer in Tandem Organic Light-Emitting Diodes: The Effect of Interfacial Energy Level and Charge Carrier Mobility. *J. Mater. Chem.* **2011**, *21*, 15332−15336.
(29) Yoo, S.; Domercq, B.; Kippelen, B. Efficient Thin-Film Organic Solar Cells Based on Pentacene/C-60 Heterojunctions. *Appl. Phys. Lett.* **2004**, *85*, 5427−5429.
(30) Liao, L.-S.; Slusarek, W. K.; Hatwar, T. K.; Ricks, M. L.; Comfort, D. L. Tandem Organic Light-Emitting Mode Using Hexaazatriphenylene Hexacarbonitrile in the Intermediate Connector. *Adv. Mater.* **2008**, *20*, 324−329.
(31) Fung, M. K.; Lau, K. M.; Lai, S. L.; Law, C. W.; Chan, M. Y.; Lee, C. S.; Lee, S. T. Charge Generation Layer in Stacked Organic Light-Emitting Devices. *J. Appl. Phys.* **2008**, *104*, 034509.
(32) Chen, C. W.; Hsieh, P. Y.; Chiang, H. H.; Lin, C. L.; Wu, H. M.; Wu, C. C. Top-Emitting Organic Light-Emitting Devices Using Surface-Modified Ag Anode. *Appl. Phys. Lett.* **2003**, *83*, 5127−5129.
(33) Hung, L. S.; Tang, C. W.; Mason, M. G.; Raychaudhuri, P.; Madathil, J. Application of an Ultrathin Lif/Al Bilayer in Organic Surface-Emitting Diodes. *Appl. Phys. Lett.* **2001**, *78*, 544−546.
(34) Zhou, X.; Blochwitz, J.; Pfeiffer, M.; Nollau, A.; Fritz, T.; Leo, K. Enhanced Hole Injection into Amorphous Hole-Transport Layers of Organic Light-Emitting Diodes Using Controlled P-Type Doping. *Adv. Funct. Mater.* **2001**, *11*, 310−314.
(35) Small, C. E.; Tsang, S.-W.; Kido, J.; So, S. K.; So, F. Origin of Enhanced Hole Injection in Inverted Organic Devices with Electron Accepting Interlayer. *Adv. Funct. Mater.* **2012**, *22*, 3261−3266.
(36) Kim, Y.-K.; Kim, J. W.; Park, Y. Energy Level Alignment at a Charge Generation Interface between 4,4′-Bis(N-Phenyl-1-Naphthylamino)Biphenyl and 1,4,5,8,9,11-Hexaazatriphenylene-Hexacarbonitrile. *Appl. Phys. Lett.* **2009**, *94*, 063305.
(37) Kim, J. H.; Yun, S. W.; An, B. K.; Han, Y. D.; Yoon, S. J.; Joo, J.; Park, S. Y. Remarkable Mobility Increase and Threshold Voltage Reduction in Organic Field-Effect Transistors by Overlaying Discontinuous Nano-Patches of Charge-Transfer Doping Layer on Top of Semiconducting Film. *Adv. Mater.* **2013**, *25*, 719−724.
(38) Li, Y.; Liu, Q.; Cai, J.; Li, Y.; Shi, Y.; Wang, X.; Hu, Z. Remarkable Reduction in the Threshold Voltage of Pentacene-Based Thin Film Transistors with Pentacene/Cupc Sandwich Configuration. *AIP Adv.* **2014**, *4*, 067126.
(39) Qi, Y.; Sajoto, T.; Kroeger, M.; Kandabarow, A. M.; Park, W.; Barlow, S.; Kim, E.-G.; Wielunski, L.; Feldman, L. C.; Bartynski, R. A.; Bredas, J.-L.; Marder, S. R.; Kahn, A. A Molybdenum Dithiolene Complex as P-Dopant for Hole-Transport Materials: A Multitechnique Experimental and Theoretical Investigation. *Chem. Mater.* **2010**, *22*, 524−531.
(40) Sakanoue, T.; Fujiwara, E.; Yamada, R.; Tada, H. Visible Light Emission from Polymer-Based Field-Effect Transistors. *Appl. Phys. Lett.* **2004**, *84*, 3037−3039.
(41) Namdas, E. B.; Ledochowitsch, P.; Yuen, J. D.; Moses, D.; Heeger, A. J. High Performance Light Emitting Transistors. *Appl. Phys. Lett.* **2008**, *92*, 183304.
(42) Sun, H.; Guo, Q.; Yang, D.; Chen, Y.; Chen, J.; Ma, D. High Efficiency Tandem Organic Light Emitting Diode Using an Organic Heterojunction as the Charge Generation Layer: An Investigation into the Charge Generation Model and Device Performance. *ACS Photonics* **2015**, *2*, 271−279.
(43) Ullah, M.; Tandy, K.; Yambem, S. D.; Muhieddine, K.; Ong, W. J.; Shi, Z.; Burn, P. L.; Meredith, P.; Li, J.; Namdas, E. B. Efficient and Bright Polymer Light Emitting Field Effect Transistors. *Org. Electron.* **2015**, *17*, 371−376.
(44) Muhieddine, K.; Ullah, M.; Maasoumi, F.; Burn, P. L.; Namdas, E. B. Hybrid Area-Emitting Transistors: Solution Processable and with High Aperture Ratios. *Adv. Mater.* **2015**, *27*, 6677−6682.
(45) Song, L.; Hu, Y.; Li, D.; Chen, H.; Liu, X. Pixeled Electroluminescence from Multi Layer Heterostructure Organic Light-Emitting Transistors. *J. Phys. Chem. C* **2015**, *119*, 20237−20243.
(46) Madigan, C. F.; Lu, M. H.; Sturm, J. C. Improvement of Output Coupling Efficiency of Organic Light-Emitting Diodes by Backside Substrate Modification. *Appl. Phys. Lett.* **2000**, *76*, 1650−1652.
(47) Namdas, E. B.; Hsu, B. B. Y.; Liu, Z.; Lo, S.-C.; Burn, P. L.; Samuel, I. D. W. Phosphorescent Light-Emitting Transistors: Harvesting Triplet Excitons. *Adv. Mater.* **2009**, *21*, 4957−4961.
(48) Schwabegger, G.; Ullah, M.; Irimia-Vladu, M.; Baumgartner, M.; Kanbur, Y.; Ahmed, R.; Stadler, P.; Bauer, S.; Sariciftci, N. S.; Sitter, H. High Mobility, Low Voltage Operating C-60 Based N-Type Organic Field Effect Transistors. *Synth. Met.* **2011**, *161*, 2058−2062.
(49) Tewari, A.; Gandla, S.; Pininti, A. R.; Karuppasamy, K.; Boehm, S.; Bhattacharyya, A. R.; McNeill, C. R.; Gupta, D. High-Mobility and Low-Operating Voltage Organic Thin Film Transistor with Epoxy Based Siloxane Binder as the Gate Dielectric. *Appl. Phys. Lett.* **2015**, *107*, 103302.
(50) Kumar, B.; Kaushik, B. K.; Negi, Y. S. Organic Thin Film Transistors: Structures, Models, Materials, Fabrication, and Applications: A Review. *Polym. Rev.* **2014**, *54*, 33−111.
(51) Pernstich, K. P.; Haas, S.; Oberhoff, D.; Goldmann, C.; Gundlach, D. J.; Batlogg, B.; Rashid, A. N.; Schitter, G. Threshold Voltage Shift in Organic Field Effect Transistors by Dipole Monolayers on the Gate Insulator. *J. Appl. Phys.* **2004**, *96*, 6431−6438.
(52) Ullah, M.; Wawrzinek, R.; Maasoumi, F.; Lo, S.-C.; Namdas, E. B. Semitransparent and Low-Voltage Operating Organic Light-

DOI: 10.1021/acsami.6b02618
ACS Appl. Mater. Interfaces 2016, 8, 14063−14070

Emitting Field-Effect Transistors Processed at Low Temperatures. *Adv. Opt. Mater.* **2016**, DOI: 10.1002/adom.201600050.

DOI: 10.1021/acsami.6b02618
ACS Appl. Mater. Interfaces 2016, 8, 14063−14070